



Phytosterol-mediated glycosomes combined with peppermint oil enhance transdermal delivery of lappaconitine by modulating the lipid composition of the stratum corneum

Hang Ruan¹ · Lina Shen¹ · Xiaolin Hou¹ · Jiaqi Li¹ · Teng Guo¹ · Chunyun Zhu¹ · Nianping Feng¹ · Yongtai Zhang¹ 

Accepted: 18 May 2023 / Published online: 15 July 2023
© Controlled Release Society 2023

Abstract

Although the introduction of glycosomes has enriched strategies for efficient transdermal drug delivery, the inclusion of cholesterol as a membrane stabilizer has limited their clinical application. The current study describes the development and optimization of a new type of glycosome (S-glycosome) that is formed in glycerol solution with β -sitosterol as the stabilizer. Moreover, the transdermal permeation properties of lappaconitine (LA)-loaded S-glycosomes and peppermint oil (PO)-mediated S-glycosomes (PO-S-glycosomes) are evaluated, and the lipid alterations in the stratum corneum are analyzed via lipidomics. The LA-loaded S-glycosomes prepared by the preferred formulation from the uniform design have a mean size of 145.3 ± 7.81 nm and an encapsulation efficiency of $73.14 \pm 0.35\%$. Moreover, the addition of PO positively impacts transdermal flux, peaking at 0.4% (w/v) PO. Tracing of the fluorescent probe P4 further revealed that PO-S-glycosomes penetrate deeper into the skin than S-glycosomes and conventional liposomes. Additionally, treatment with PO-S-glycosomes alters the isoform type, number, and composition of sphingolipids, glycerophospholipids, glycerolipids, and fatty acids in the stratum corneum, with the most notable effect observed for ceramides, the main component of sphingolipids. Furthermore, the transdermal administration of LA-loaded PO-S-glycosomes improved the treatment efficacy of xylene-induced inflammation in mice without skin irritation. Collectively, these findings demonstrate the feasibility of β -sitosterol as a stabilizer in glycosomes. Additionally, the inclusion of PO improves the transdermal permeation of S-glycosomes, potentially by altering the stratum corneum lipids.

Keywords β -Sitosterol · Ethosomes · Liposomes · Lipidomics · Arthritis · Transdermal

Introduction

Lappaconitine (LA) is a monoester diterpene alkaloid isolated from the root of *Aconitum sinomontanum* Nakai (family Ranunculaceae), which has shown promise for its anti-inflammatory and analgesic effects [1]. However, LA is insoluble in water, poorly absorbed orally, has a short biological half-life, and is irritating to the gastrointestinal

tract, making it unfavorable for oral administration, and transdermal delivery is an effective way to avoid its shortcomings [2].

Liposomes with deformable properties, including transfersomes, niosomes, ethosomes, glycosomes, and invasomes, have been widely reported as carriers for enhanced transdermal drug delivery. In particular, ethosomes are transdermal delivery nanocarriers that were first reported by Horwitz et al. in 1999 [3]. This nanosystem generally comprises 10~40% (v/v) short-chain alcohols, including ethanol, glycerol, propylene glycol, and isopropanol, which soften the phospholipid membrane, increase the solubility of lipid-soluble drugs, and improve nanocarrier drug loading [4, 5]. Moreover, short-chain alcohols can improve transdermal permeation [6]. However, conventional ethanol-containing ethosomes have poor stability due to the volatility of ethanol and can cause skin irritation. To circumvent these issues, the ethanol in ethosomes has been replaced

✉ Chunyun Zhu
zhuchunyun@126.com

✉ Nianping Feng
npfeng@shutcm.edu.cn

✉ Yongtai Zhang
analysisdrug@126.com

¹ Department of Pharmaceutics, Shanghai University of Traditional Chinese Medicine, Shanghai 201203, China

with glycerol to form “glycosomes,” providing improved physical stability and biocompatibility [7].

Cholesterol is commonly employed as a membrane stabilizer in liposomes. This amphiphilic small molecule is interspersed between phospholipids within membranes, where it functions to maintain a relatively stable liquid crystal state [8]. However, excess cholesterol is reportedly associated with inflammation and activation of innate immune responses [9]. As such, cholesterol-containing preparations are not recommended for patients requiring restricted cholesterol intake, thus limiting the clinical application of liposomal drugs. Meanwhile, phytosterols are derivatives of perhydrocyclopentanophenanthrene with a structure similar to that of cholesterol, which possess anti-cancer, anti-inflammatory, and cholesterol-lowering properties, while also serving to increase the stability of liposome membranes [10–12]. β -Sitosterol is a natural plant-derived ingredient that has been widely used in the pharmaceutical industry and has exhibited cholesterol-lowering and tissue repair properties [13]. Previous reports have shown that the size of liposomes formed with soybean lecithin and β -sitosterol differs by < 40% compared to those formed with cholesterol after storage for 3 weeks. Furthermore, phytosterols significantly increase retinol stability in liposomes [14, 15].

Volatile oils extracted from plants in the Asteraceae, Rutaceae, Umbelliferae, Lamiaceae, Zingiberaceae, and Magnoliaceae families have been served as permeation enhancers [16]. Additionally, some volatile oils have the properties of increasing subcutaneous microcirculation, thereby speeding up drug transport in the skin and increasing the efficiency of transdermal drug penetration [17–19]. In this study, peppermint oil was employed for improving transdermal permeation of LA.

The current study seeks to develop a novel cholesterol-free glycosome with β -sitosterol as the stabilizer and glycerol as the membrane softener (S-glycosomes) (Fig. 1). The transdermal permeation properties of S-glycosomes and peppermint oil (PO)-mediated S-glycosomes (PO-S-glycosomes)

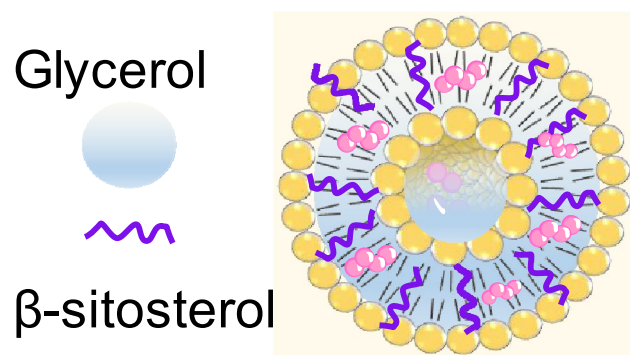


Fig. 1 Composition of S-glycosomes

carrying the anti-inflammatory active ingredient lappaconitine (LA) were evaluated, and lipid alterations in the stratum corneum (SC) were analyzed by lipidomics. The novel platform described in this study has the potential to improve liposome-associated drug solubility and enhance transdermal permeability.

Materials and methods

Materials

LA (purity > 98%) was purchased from Yuanye Biotechnology Co., Ltd. (Shanghai, China). Hydrogenated soybean phosphatidylcholine (HSPC) was purchased from AVT Shanghai Pharmaceutical Tech Co., Ltd. Soybean phosphatidylcholine (SPC-100; soybean lecithin content: 100%) and β -sitosterol (purity > 75%) were purchased from Macklin Biochemical Technology Co., Ltd. (Shanghai, China). PO was purchased from Aladdin Biochemical Technology Co., Ltd. (Shanghai, China). The P4 fluorescence probe was gifted by prof. Wu Wei from the School of Pharmacy, Fudan University. Additionally, the SAKURA Tissue-Tek O.C.T. compound was purchased from Sakura Finetek Japan Co., Ltd. (Tokyo, Japan), DAPI solution (ready use 10 μ g/mL) from MeilunBio Co., Ltd. (Dalian, China), and 10% neutral formalin from Ruiyu Biotechnology Co., Ltd. (Shanghai, China). All other chemicals were procured from Sinopharm Chemical Reagent Co., Ltd. (Shanghai, China).

Animals

Specific pathogen-free, male BALB/c mice (6–8 weeks, 22 ± 2 g) were supplied by the Animal Experiment Center of Shanghai University of Traditional Chinese Medicine. The animals were housed in a controlled atmosphere with $55 \pm 10\%$ relative humidity at a temperature of 23 ± 2 °C. All animal experiments were performed according to the relevant regulations of the Experimental Animal Welfare and Ethics Committee of Shanghai University of Traditional Chinese Medicine (Approval No.: PZSHUTCM2304140001). The experiments were carried out after 1 week of adaptive feeding.

High-performance liquid chromatography (HPLC) analysis of LA

LA was analyzed via HPLC (LC-2010AHT, Shimadzu Corporation, Kyoto, Japan) with a C18 chromatographic column (4.6×250 mm, 5 μ m; Dikma Technologies Inc., Beijing, China) at a detection wavelength of 252 nm. The mobile phase was a mixture of acetonitrile and ultrapure water (0.3% triethylamine adjusted to pH 8.0 with phosphoric acid) (80:20, v/v). Different concentrations of LA

(10 μL) were injected and analyzed at a 1 mL/min flow rate and column temperature of 30 °C. The linear regression equation, with LA concentration as the independent variable and peak area as the dependent variable, was $y = 13.654x + 2.351$, $r = 0.9997$. A good linear relationship was detected between the LA concentration and peak area in the range of 1.00–100.00 $\mu\text{g LA/mL}$. The limit of detection was 0.50 $\mu\text{g LA/mL}$, and the limit of quantitation was 1.00 $\mu\text{g LA/mL}$.

Preparation of S-glycosomes and the compared preparations

LA-loaded S-glycosomes were prepared using film dispersion combined with ultrasonication. Briefly, LA (20 mg), SPC-100 (80 mg), and β -sitosterol (4 mg) were dissolved in 4 mL of mixed solvents (methanol:trichloromethane = 1:2, v/v). The organic solvents were removed to obtain uniform thin lipid films with a rotary evaporator (RE-2000A, Yarong Biochemical Instruments Co., Ltd., Shanghai, China). The lipid films were hydrated with 4 mL of 10% (w/v) glycerol-water solution for 2 h at 40 °C. For preparing PO-containing S-glycosomes (PO-S-glycosomes), peppermint oil was dispersed in the hydration solution. The obtained mixture was subjected to probe ultrasound (SCIENTZ-IIID, Xinzhi Biotechnology Co., Ltd., Ningbo, China) in an ice bath for 6 min (power: 20%, interval time: 5 s) to form the final S-glycosomes.

The compared liposomes were prepared by using similar method described as preparing S-glycosomes; however, pure water replaced the glycerol-water solution in the hydration process. Additionally, the compared LA solution (Free LA) was prepared by dissolving LA in 20% PEG 400 (v/v) water solution [20]. Notably, the LA concentration in all tested preparations was 0.5% (w/v) for in vitro transdermal, and in vivo anti-inflammatory, evaluations.

The effect of SPC-100 and glycerol content on the size distribution and EE of the S-glycosomes formed was investigated separately, keeping all other conditions constant. Further, a uniform design array $U_7(7^3)$ was used to preferably select the formulation composition, with glycerol content (X_1), SPC-100 content (X_2), and the drug to phospholipid (SPC-100) weight ratio (X_3) set as variable factors, and drug loading (DL), EE, and size distribution were used as evaluation responses. The experiments were conducted in triplicate.

Characterization of LA-loaded S-glycosomes

The LA-loaded S-glycosomes and PO-S-glycosomes were diluted 20 times with ultrapure water, and the size distribution was measured using Malvern Autosizer Nano ZS90 (Malvern Instruments Ltd., Malvern, UK) at 25 °C and a

dynamic light scattering angle of 90°. The zeta potential values were measured by the same instrument; however, the test samples were not diluted prior to testing. All of the above measurements were performed in triplicate.

In addition, the nano-dispersions were dropped onto a 400-mesh copper mesh, stained with 2% phosphotungstic acid solution for 3 min, and observed with a JEM-1400 Flash transmission electron microscope instrument (JEOL Ltd., Tokyo, Japan). The pH values of the final preparations were measured by using a PHS-25 pH meter (Shanghai Yidian Scientific Instrument Co., Ltd., Shanghai, China).

Encapsulation efficiency (EE) and drug loading (DL) capacity

Five hundred microliter of the LA-loaded S-glycosomes and PO-S-glycosomes was, respectively, diluted 10 times with ultrapure water, then was put into an ultrafiltration centrifuge tube with a molecular weight cut-off of 30 kD, and centrifuged at $7853 \times g$ for 10 min, the filter cake was washed twice with 0.1 mL of pure water per time, and the free drug (W_f) was separated in the collected filtrate. The total drug in LA-loaded S-glycosomes (W_t) was extracted via washing with methanol (v/v) 20 times. The amount of LA in the samples was measured using HPLC, and the encapsulation efficiency (EE) and drug loading (DL) were calculated using Eqs. (1) and (2):

$$EE(\%) = \left(1 - \frac{W_f}{W_t}\right) \times 100 \quad (1)$$

$$DL(\%) = \frac{W_t - W_f}{W_e} \times 100 \quad (2)$$

where W_e is the total weight of the LA-encapsulated S-glycosomes.

In vitro transdermal permeation experiments

Mice were euthanized using pentobarbital sodium. Thereafter, the abdominal hair was shaved using an electric shaver, ensuring that the SC was intact. The abdominal skin was isolated, and its subcutaneous fat and tissue were eliminated.

A SYSTEM 918–12 automated transdermal diffusion cell sampling system (Logan Instruments Corp., Somerset, NJ, USA) was used to test transdermal permeability. Mice skin, with the SC facing upwards, was firmly fixed to the diffusion cell with an effective transdermal area of 1.77 cm^2 and a chamber with the volume of 12 mL, accommodating 12 mL of receiving medium (30% ethanol in pH 7.4 PBS) [21]. The receiving medium was designed to ensure adequate dissolution of the penetrating drug (meeting the sink conditions) without damaging the integrity of the skin and in addition had an antibacterial effect. One milliliter of each preparation

containing the same amount of LA was applied evenly to the donor skin. The system was maintained at 32 °C with agitation at 500 rpm, sampled at pre-determined time points, and supplemented with an equivalent volume of fresh receiving medium preheated to 32 °C. All tests were performed in triplicate, and the samples were determined using HPLC.

To visualize the transdermal permeation behavior of nanovesicles, LA was replaced with 100 µg/mL of P4 fluorescent probe-labeled S-glycosome, PO-S-glycosome, and liposome solution. Subsequently, 1 mL of each P4-labeled nanocarrier (P4 concentration: 1 µg/mL) was added to the donor skin for a preset time. The skin was then washed with normal saline, fixed in 4% paraformaldehyde for 2 h, OCT-embedded, and snap-frozen in liquid nitrogen. The tissue sections were then cut longitudinally at a thickness of 30 µm, fixed in 4% paraformaldehyde for 10 min, and stained with 10 µg/mL DAPI solution for 10 min. Finally, sections were observed (Ex/Em: DAPI, 358 nm/461 nm; P4, 645 nm/650 nm) with a Cytation5 Cell Imaging Multimode Reader (BioTek Instruments Corp., Vermont, USA).

Lipidomics analysis of the SC

The mice were randomly grouped, and their back hair was removed with an electric razor. The drug administration groups had 1 mL of the test solution (0.4% PO or 0.4% PO-S-glycosomes) evenly dripped onto a 2 cm × 4 cm cotton pad and then applied to their skin daily for 5 days, while the normal control group (normal) was untreated. Twenty-four hours after the last dose, the mice were euthanized by intraperitoneal injection of 1% sodium pentobarbital solution at 50 mg/kg, and the skin of the dosed area was immediately excised and washed with saline. The skin was then covered with pressure-sensitive tape (PE, HYNAUT) and rolled evenly to ensure adherence to the skin for 30 s. The tape was removed; the process was repeated 30 times until the tape no longer adhered to the skin [22]. SC lipids were extracted using a modified method developed by Bligh and Dyer [23, 24]. Lipids were extracted from each sample with 0.75 mL of a methanol:chloroform (1:2) solution, vortexed for 1 min, and incubated at 4 °C for 3 min. Subsequently, 0.25 mL of chloroform was added; the solutions were vortexed for 1 min, incubated at 4 °C for 5 min, washed with 0.25 mL of double distilled water, vortexed for 1 min, and incubated at 4 °C overnight. The tape was removed, the remaining solution was passed through a 0.45-µm filter membrane, and the obtained filtrate was centrifuged at 13,000 × g for 10 min (4 °C). Next, 400 µL of the lower organic layer was sampled, dried with nitrogen, treated with 100 µL of chloroform/methanol/n-butanol (1:2:4), vortexed for 3 min, and centrifuged at 13,000 × g for 10 min (4 °C). The supernatant was analyzed by LC–MS (UHPLC-Q Exactive HF-X, Thermo Fisher Scientific, 168 Third Avenue Waltham, MA

USA) with an Accucore C30 column (100 mm × 2.1 mm; i.d. 2.6 µm; Thermo Fisher Scientific); mobile phase A, 50% aqueous acetonitrile (containing 0.1% formic acid, 10 mmol/L ammonium acetate); and mobile phase B, acetonitrile:isopropanol:water = 10:88:2 (v/v/v; containing 0.02% formic acid and 2 mmol/L ammonium acetate). The column temperature was 40 °C, and the elution was carried out according to the procedure described in Table 1. The samples were subjected to electrospray ionization, and the mass spectral signals were collected in positive and negative ion scanning mode (Table 2).

In vivo anti-inflammatory analysis

BALB/c mice were randomly divided into 7 groups with 5 mice in each group, including normal, model, and treatment groups. The left ear of the mouse in each treatment group was evenly applied with the corresponding preparation at a dose of 100 mg/kg of LA once daily for 3 days [25]. One hour after the last administration, the left ear of the mouse in both the model group and each treatment group was uniformly applied with 25 µl of xylene to induce acute inflammation, with the untreated right ear served as control [26]. One hour later, the mice were euthanized, and ear flaps 8.0 mm in diameter were sampled and weighed. The weight difference between the left and the right ear flaps represented the extent of edema. The edema inhibition rates were calculated according to Eq. (3):

$$\text{Inhibition(\%)} = \left(1 - \frac{A}{B}\right) \times 100 \quad (3)$$

where *A* is the mean edema extent (difference in ear flap weight) of the treatment group and *B* is the mean edema extent (difference in ear flap weight) of the pathological model group.

Additionally, the ear samples were fixed in 10% formalin solution for 24 h. Subsequently, routine paraffin embedding and sectioning (thickness: 4 µm), as well as hematoxylin and eosin (H&E) staining, were performed. Pathological changes in skin sections were assessed by the Cytation5 Cell Imaging Multimode Reader.

Table 1 Mobile phase elution gradient

Time (min)	Flow (mL/min)	A (%)	B (%)
0	0.4	65	35
4	0.4	40	60
12	0.4	15	85
15	0.4	0	100
17	0.4	0	100
18	0.4	65	35
20	0.4	65	35

Table 2 Mass spectrometry parameters

Item	Description	Parameter
Scanning range	Scan type (m/z)	200–2000
Sheath gas	Sheath gas flow rate (psi)	60
Auxiliary heating gas	Aux gas flow rate (psi)	20
Ion source heating temperature	Aux gas heater temp (°C)	370
Ionization voltage (–)	IonSpray Voltage Floating (ESI+)(V)	+3000
Ionization voltage (+)	IonSpray Voltage Floating (ESI–)(V)	–3000
Collision energy	Normalized collision energy (V)	20–40–60

Preliminary evaluation of skin irritation

The hair on the back of the mice (6 per group) was removed, and the skin irritation of the preparation was evaluated by the comparison method between the anterior and posterior sides of the same body itself. The 0.4% PO-S-glycosomes (0.4 mL) were applied to the posterior side of the skin and massaged until complete absorption, while the anterior side of the skin was left untreated. The skin was monitored visually under natural light at 1 h after drug administration for local reactions at the drug administration site, including erythema, edema, degree, and extent of congestion, photographed, and administered for 7 consecutive days. The skin of mice on day 0 (unadministered) and day 7 (7 days of continuous administration) was removed after the animals were euthanized, paraffin-embedded, sectioned, and stained with H&E to observe the pathological changes at the site of administration.

Statistical methods

Data were analyzed by using SPSS 21.0 software (SPSS Inc., Chicago, IL, USA). Data conforming to a normal distribution

were described as mean \pm standard deviation, while differences between two groups were analyzed by Student's *t*-test, and differences between multiple groups were analyzed by one-way ANOVA. Those not conforming to normal distribution were expressed as median and interquartile spacing, and the non-parametric rank sum test Mann–Whitney test was chosen. $p < 0.05$ was considered statistically significant.

Results

Effect of glycerol and SPC-100 on LA-loaded S-glycosome characteristics

EE is an important index to evaluate S-glycosomes as smaller particle size is more conducive to transdermal permeation of nanoparticles. The concentration of glycerol and SPC-100 was investigated by single-factor analysis with EE and particle size as indexes. With an increase in SPC-100 concentration from 0.5 to 2.5%, the EE of the S-glycosomes gradually increased, while no obvious relationship was detected between SPC-100 concentration and particle

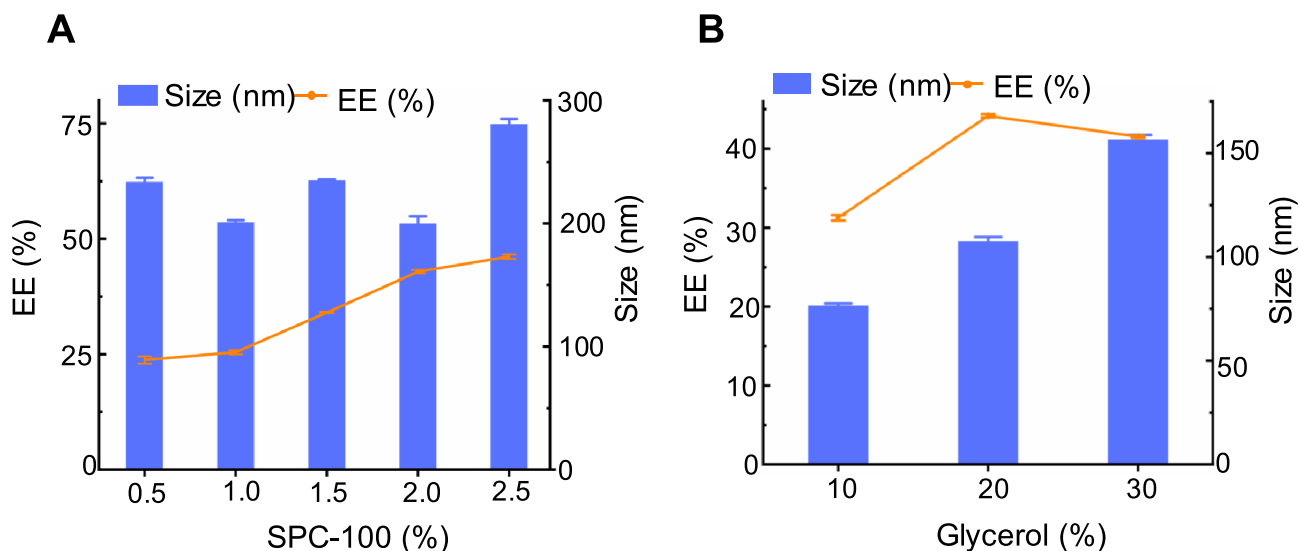


Fig. 2 Effect of **A** SPC-100 and **B** glycerol concentrations on the particle size and encapsulation efficiency of LA-loaded S-glycosome. EE, encapsulation efficiency. Values represented as the mean \pm standard deviation ($n=3$)

Table 3 S-glycosome formulations with different influencing factors and responses in $U_7(7^3)$ uniform design experiments

Formulation No	Influencing factor			Response		
	X_1 (w/v, %)	X_2 (w/v, %)	X_3 (w/w, %)	EE (%)	DL (%)	Size (nm)
1	10.00	1.00	12.50	22.72 ± 1.31	0.03 ± 0.02	152.70 ± 1.12
2	15.00	2.00	5.00	15.22 ± 0.44	0.35 ± 0.01	193.27 ± 1.46
3	20.00	3.00	16.67	63.19 ± 1.18	6.64 ± 0.12	206.67 ± 1.52
4	25.00	0.50	6.25	47.79 ± 1.97	1.51 ± 0.06	190.97 ± 13.39
5	30.00	1.50	25.00	21.55 ± 5.25	2.26 ± 0.55	300.70 ± 8.75
6	40.00	2.50	8.33	24.35 ± 0.13	1.85 ± 0.01	377.00 ± 3.32
7	50.00	3.50	4.00	4.89 ± 0.04	0.12 ± 0.00	394.13 ± 14.66

X_1 glycerol content, X_2 phospholipid content, X_3 drug to phospholipid weight ratio, *EE* encapsulation efficiency, *DL* drug loading, *Size* particle size

size (Fig. 2). Meanwhile, with an increase in glycerol concentration from 10 to 30%, the S-glycosome particle size gradually increased ($p < 0.0001$), whereas the EE initially increased and then decreased.

Uniform design for optimized S-glycosome formulation

On the basis of single-factor testing, $U_7(7^3)$ uniform design was selected to evaluate the interaction of three factors, namely, glycerol content (X_1), phospholipid content (X_2), and the drug to phospholipid (SPC-100) weight ratio (X_3), using EE, DL, and particle size as the evaluation responses (Table 3). Polynomial stepwise regression analysis was performed, and the three regression equations for EE, DL, and particle size were obtained (Table 4). Variance analysis was conducted on the fitted regression equations to obtain the *t*-value and *p*-value of significance for each phase coefficient. The obtained *p*-value was < 0.05 , indicating that each factor had a significant influence on the responses. The R^2 and adjusted R^2 of the three regression equations were between 85 and 100%, with a higher value reflecting superior model fitting. The positive and negative coefficients for each factor in the equation corresponded to the synergistic and antagonistic effects of factors on the responses, respectively.

Equation (4) revealed that the interaction between phospholipid content and drug to phospholipid weight ratio had

significant positive effects on EE. This might be related to the lipophilicity of LA which could be more encapsulated in the lipid phase with an increase in phospholipid content. This was consistent with the single-factor tests for the effect of phospholipid concentration on EE. In addition, the EE increased with an increase in the drug to phospholipid ratio, which might be due to the integration between LA and phospholipid being closer to the phospholipid saturation value [27].

Equation (5) revealed that the phospholipid content, drug to phospholipid ratio, and their interaction significantly impacted DL. Meanwhile, Eq. (6) showed that glycerol concentration could significantly affect S-glycosome particle size, which was positively correlated with glycerol content. This was consistent with the results of the single-factor investigation for glycerol concentration. This may have been caused by the viscosity of the glycerol, allowing it to interact with phospholipids and decrease the S-glycosome membrane rigidity [28].

The optimal ratio of each factor in the equations was determined by maximizing EE and DL and minimizing the particle size. Finally, the optimized formulation was obtained: glycerol concentration of 10% (w/v); SPC-100 concentration of 2% (w/v); a drug to phospholipid ratio of 25% (w/w), with 0.1% (w/v) β -sitosterol; and a theoretical response value particle size of 146.34 nm, EE of 75.81%, and DL of 5.10%. Three batches of S-glycosomes were prepared according to the optimized formulation, and the

Table 4 Regression analysis for encapsulation efficiency, drug loading, and particle size

Regression equation	<i>t</i> -value	<i>p</i> -value	R^2	Adj R^2
$Ee = 1.58 + 3.525 \times X_1 - 0.917 \times X_1 \times X_2 + 2.238 \times X_2 \times X_3 - 0.1488 \times X_1 \times X_3(4)$	$t X_1 = 4.44$ $t X_1 X_2 = -5.15$ $t X_2 X_3 = 6.03$ $t X_1 X_3 = -4.99$	$p X_1 = 0.047$ $p X_1 X_2 = 0.036$ $p X_2 X_3 = 0.026$ $p X_1 X_3 = 0.038$	95.78%	87.35%
$DL = 3.548 - 1.832 \times X_2 - 0.3980 \times X_3 + 0.3034 \times X_2 \times X_3(5)$	$t X_2 = -5.42$ $t X_3 = -5.85$ $t X_2 X_3 = 9.02$	$p X_2 = 0.012$ $p X_3 = 0.010$ $p X_2 X_3 = 0.003$	97.85%	95.70%
$Size = 80.4 + 6.594 \times X_1(6)$	$t X_1 = 7.16$	$p X_1 = 0.010$	91.12%	89.35%

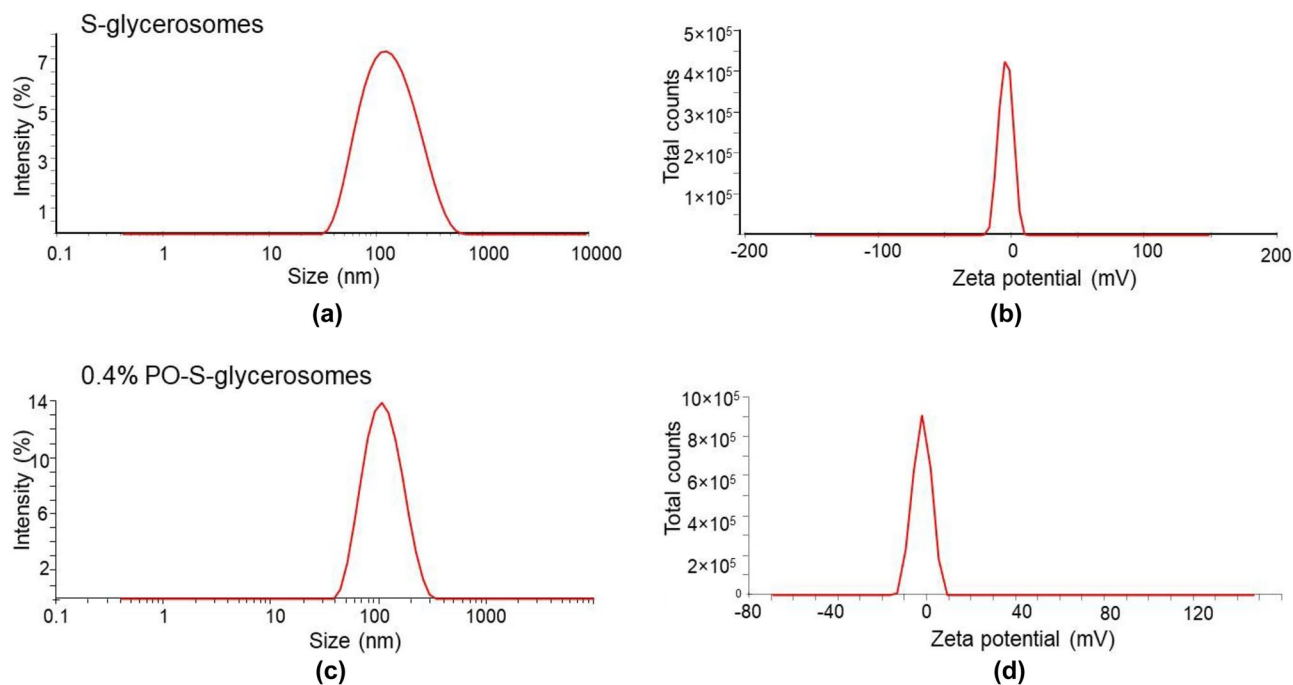


Fig. 3 Profiles of size distribution **a, c** and zeta potential **b, d** of LA-loaded S-glycrosomes and 0.4% PO-S-glycrosomes

average particle size of LA-loaded S-glycrosomes was 145.30 ± 7.81 nm, PDI was 0.277 ± 0.045 , zeta potential was -4.33 ± 1.00 mV (Fig. 3a, b), EE was $73.14 \pm 0.35\%$, and DL was $4.40 \pm 1.91\%$. These results are similar to the predictions made for the uniform design, thus confirming the reliability of the optimized formulation for S-glycrosomes. The PO-S-glycrosome dispersion system with a PO concentration of 0.4% (v/v) (0.4% PO-S-glycrosomes) prepared with the preferred formulation composition of S-glycrosomes had a mean particle size, PDI, and zeta potential values of 100.09 ± 0.53 nm, 0.25 ± 0.07 , and -2.67 ± 0.27 mV (Fig. 3c, d) and EE and DL of $74.80 \pm 1.5\%$ and $5.26 \pm 0.30\%$, respectively.

The LA-loaded S-glycrosomes prepared with the optimized formulation are homogeneous dispersions presenting a suspension (Fig. 4A) with a pronounced Tyndall phenomenon (Fig. 4B). The unloaded vesicles in the transmission

electron microscopic field showed a clear multilayer structure with a transparent inner cavity (Fig. 4C), while the drug-loaded vesicles were bright white, and the fine structure was difficult to distinguish, suggesting that the drug molecules were distributed in the phospholipid bilayers and the inner cavity (Fig. 4D).

PO-S-glycrosomes exhibit superior transdermal permeation

To investigate the effects of different proportions of PO on in vitro transdermal permeability, PO-S-glycrosomes with various PO concentrations, S-glycrosomes, liposomes, and free LA were, respectively, applied to isolated mice skin. The cumulative permeation amounts of LA released by nanocarrier groups were higher than that of the free LA ($p < 0.0001$) (Fig. 5A). Regarding the nanocarrier groups,

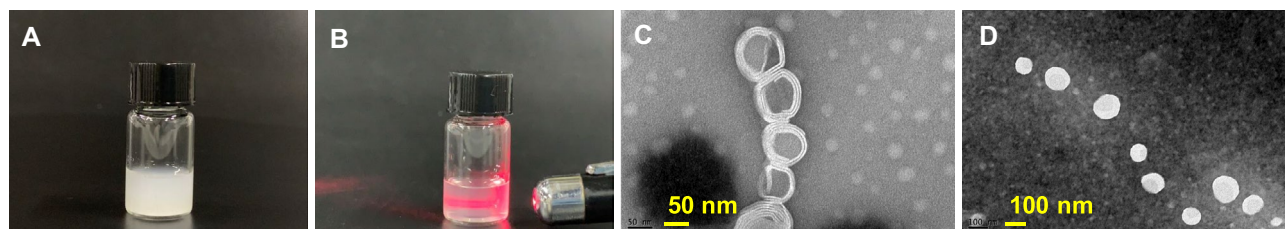


Fig. 4 Appearance of LA-loaded glycosome dispersion **A**; Tyndall phenome **B** (diluted with 7×volume water); and transmission electron micrograph of the glycosomes (**C** empty glycosomes and **D** LA-loaded glycosomes)

the S-glycosomes exhibited greater performance in the cumulative transdermal release of LA than the liposomes ($p < 0.001$). In the PO-S-glycosome groups, as the content of PO increased, cumulative permeation exhibited a parabolic trend, first increasing and then decreasing. However, the optimal permeation enhancing effect was observed following application of 0.4% PO (0.4% PO-S-glycosome), and the cumulative permeation amount at 24 h was $26.96 \mu\text{g}/\text{cm}^2$, 1.68-fold greater than that of S-glycosomes (without PO) and 3.10-fold greater than that of free LA. As the concentration of PO continued to increase, the 24-h cumulative permeation amount of S-glycosomes with 0.8% PO (0.8% PO-S-glycosome) decreased to $23.57 \mu\text{g}/\text{cm}^2$, which was 1.47-fold greater than that of S-glycosomes and 2.72-fold greater than that of free LA. The cumulative permeation amount of 1.5% PO (1.5% PO-S-glycosome) was $11.43 \mu\text{g}/\text{cm}^2$, lower than that of the S-glycosome and liposome groups and only 1.31-fold greater than that of free LA. These results indicated that low concentrations of PO in S-glycosomes enhanced permeation, while high concentrations decreased transdermal delivery of LA.

Both S-glycosomes and liposomes accelerated the transdermal flux of LA (Fig. 5B); however, the permeation effect of S-glycosomes was better ($p < 0.05$). Moreover, increased PO concentration in S-glycosomes from 0.1 to 0.4% led to an increase in transdermal flux. The 0.4% PO-S-glycosomes exhibited optimal transdermal flux ($p < 0.0001$), which was 3.17-fold greater than that of free LA and 1.69-fold greater than that of S-glycosomes. However, the increasing trend reversed at PO concentration from 0.8 to 1.5%.

P4, a pH-insensitive fluorescent probe that quenches rapidly in water, was used to label the phospholipid vesicles under test and then to assess the properties and pathways of nano-carrier penetration into the skin by tracking the distribution

of P4 fluorescence [29, 30]. In this way, PO-S-glycosomes, S-glycosomes, and liposomes were found to penetrate the skin (Fig. 6), with the fluorescence intensity increasing over time. The PO-S-glycosome and S-glycosome groups exhibited higher fluorescence intensity than liposomes, with PO-S-glycosomes in particular showing the strongest fluorescence intensity following 2 h of treatment. Thus, PO was determined to be an excellent penetration enhancer. Meanwhile, the fluorescence in the liposome group was primarily retained within the epidermis and hair follicles after 4 h of treatment, while that in the PO-S-glycosome and S-glycosome groups were widely distributed throughout the epidermis, hair follicles, and dermis. Thus, the rigid liposomes failed to enter the dermis, while the flexible S-glycosomes penetrated into the deeper layers of the skin, an effect that was further enhanced by PO.

PO-S-glycosome treatment alters the lipid composition and content of the SC

The lipidomic results identified 614 differential lipids in the SC of the three groups and significant differences in lipids between the groups (Fig. 7A). Treatment with PO or PO-S-glycosomes altered the isoform type, number, and content of sphingolipids (SPs), glycerophospholipids (GPs), glycerolipids (GLs), and fatty acids (FAs) in the SC compared to the normal group (Fig. 7B); this effect was the most pronounced for SP, of which ceramides (CER) are a major constituent. More specifically, the PO and PO-S-glycosome groups contained 116 and 68 differential CER isoforms in the SC, respectively, compared to the non-treated group. Meanwhile, treatment with PO and PO-S-glycosomes resulted in the presence of only three and one differential FA isoforms, respectively, and treatment with PO-S-glycosomes markedly altered the GP and GL isoforms in the SC. However, the PO group showed the greatest difference in GPs compared

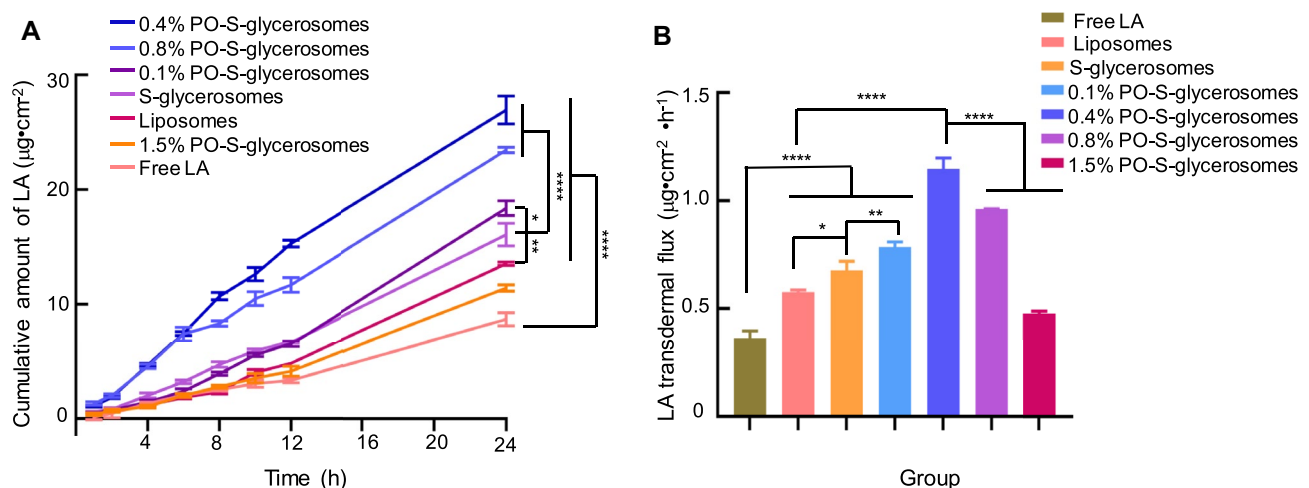


Fig. 5 In vitro cumulative transdermal profiles **A** and transdermal fluxes **B** of LA. Values represented as the mean \pm standard deviation ($n = 3$). **** $p < 0.0001$, *** $p < 0.0001$, ** $p < 0.01$, * $p < 0.05$

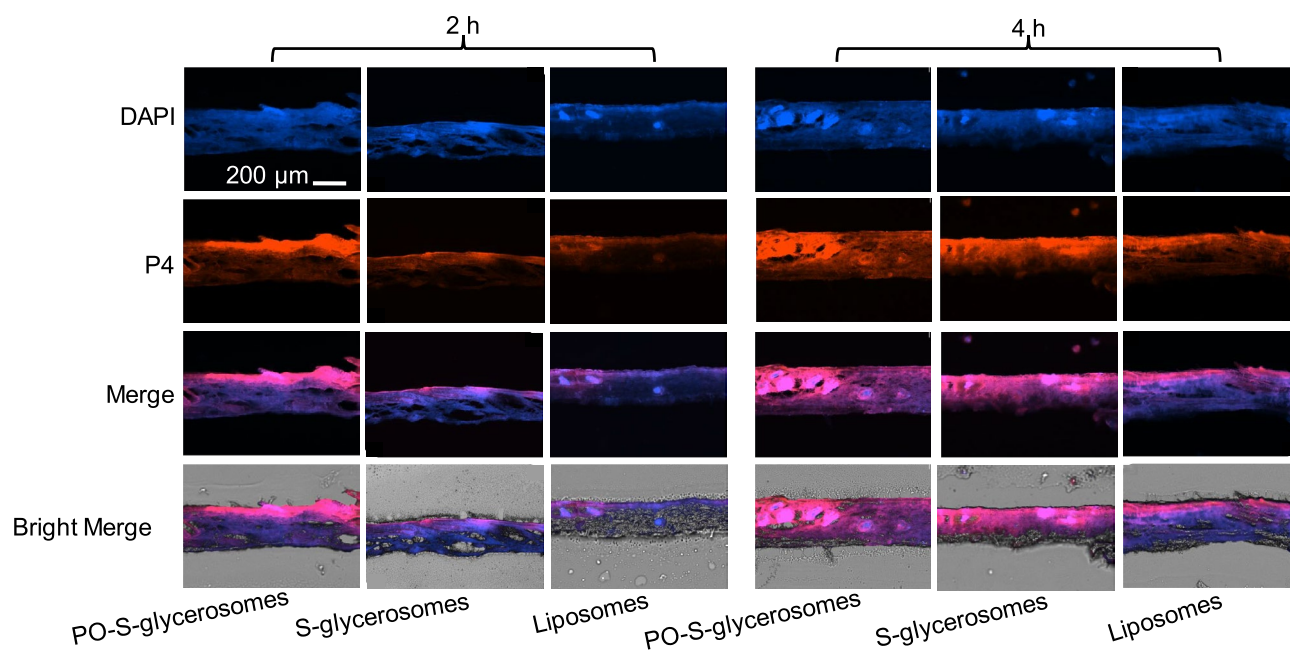


Fig. 6 Fluorescence distribution in the mouse skin after being treated with P4-labeled PO-S-glycerosomes, S-glycerosome, and liposomes for 2 h and 4 h, respectively, imaged by Cytation-5 Live Cell Imaging System (Ex/Em: DAPI, 358 nm/461 nm; P4, 645 nm/650 nm)

to the PO-S-glycerosome group. One-way ANOVA yielded 25 differential ceramide isoforms among the groups (Fig. 8), namely, Cer (d18:1/14:0), Cer (d18:1/16:0), Cer (d18:1/17:1), Cer (d18:1/18:1), Cer (d18:1/18:2), Cer (d18:1/20:1), Cer (d18:1/24:2), Cer (d18:2/16:0), Cer (d19:2/18:1), Cer (d19:2/22:0+O), Cer (d24:1/17:0+O), Cer (d24:1/18:0+2O), Cer (m17:1/16:0+O), Cer (m21:0/17:1), Cer (m22:0/17:1), Cer (t17:0/23:0+O), Cer (t17:0/24:1), Cer (t17:0/25:0+O), Cer (t18:0/16:1), Cer (t18:0/22:0+O), Cer (t18:0/23:2), Cer (t18:0/24:0), Cer (t18:1/16:0+O), Cer (t18:1/21:0), and Cer (t18:1/24:0+O). That is, the addition of PO significantly upregulated the abundance of the above ceramides as well as glycerolipid diacylglycerol (DG) (8:1e/10:1), glycerophospholipid phosphatidylcholine (PC) (15:0/16:0), and lysophosphatidylethanolamine (LPE) (18:0) in the SC. In addition, both PO and PO-S-glycerosomes upregulated the glycerolipid triacylglycerol (TG) (18:2e/10:1/10:1), TG (11:0/9:0/18:2), and TG (20:5/20:5/20:5) and downregulated TG (18:2e/8:0/11:0), TG (15:0/16:0/16:1), and TG (16:1e/9:0/9:0) abundance in the SC (Fig. 9). These findings provide insights into the potential mechanism by which the newly designed nanocarriers enhance skin permeability.

PO-S-glycerosomes exhibit superior anti-inflammation effects in vivo

Xylene induces ear edema in mice by promoting vasodilation and increasing vascular permeability, mimicking edema in the early stages of acute inflammation [31]. The model group had red and swollen ears with subcutaneous congestion,

vasodilatation, tissue edema, and a small amount of inflammatory cell infiltration, with significantly thickened ear tissue. Following free LA treatment, the redness and swelling slightly subsided, with a small amount of congestion and edema. The edema was relatively absent following treatment with LA-loaded liposomes and S-glycerosomes, and the thickness of the ear tissue decreased significantly following PO addition (Fig. 10).

Treatment with free LA inhibited xylene-induced ear edema (Fig. 11), however, to a significantly lesser extent than the nanocarrier groups ($p < 0.0001$). The proportion of ear edema inhibition in each nanocarrier group paralleled the in vitro transdermal flux results, excluding the 0.8% PO-S-glycerosome group, which did not significantly reduce ear edema ($87.18 \pm 1.34\%$) compared to the 0.4% PO-S-glycerosomes. Nevertheless, PO mediation significantly increased the inhibition percentage of ear edema and exhibited a better anti-inflammatory effect ($p < 0.0001$). However, the increased inhibition slowed with an increase in PO concentration, possibly indicating that a relatively high concentration of PO hinders the transdermal permeation of LA from S-glycerosomes.

Preliminary skin irritation

After 7 consecutive days of 0.4% PO-S-glycerosome administration, the skin showed no pathological changes such as erythema or blotchiness, no edema of the skin tissue, and no inflammatory cell infiltration (Fig. 12), indicating that

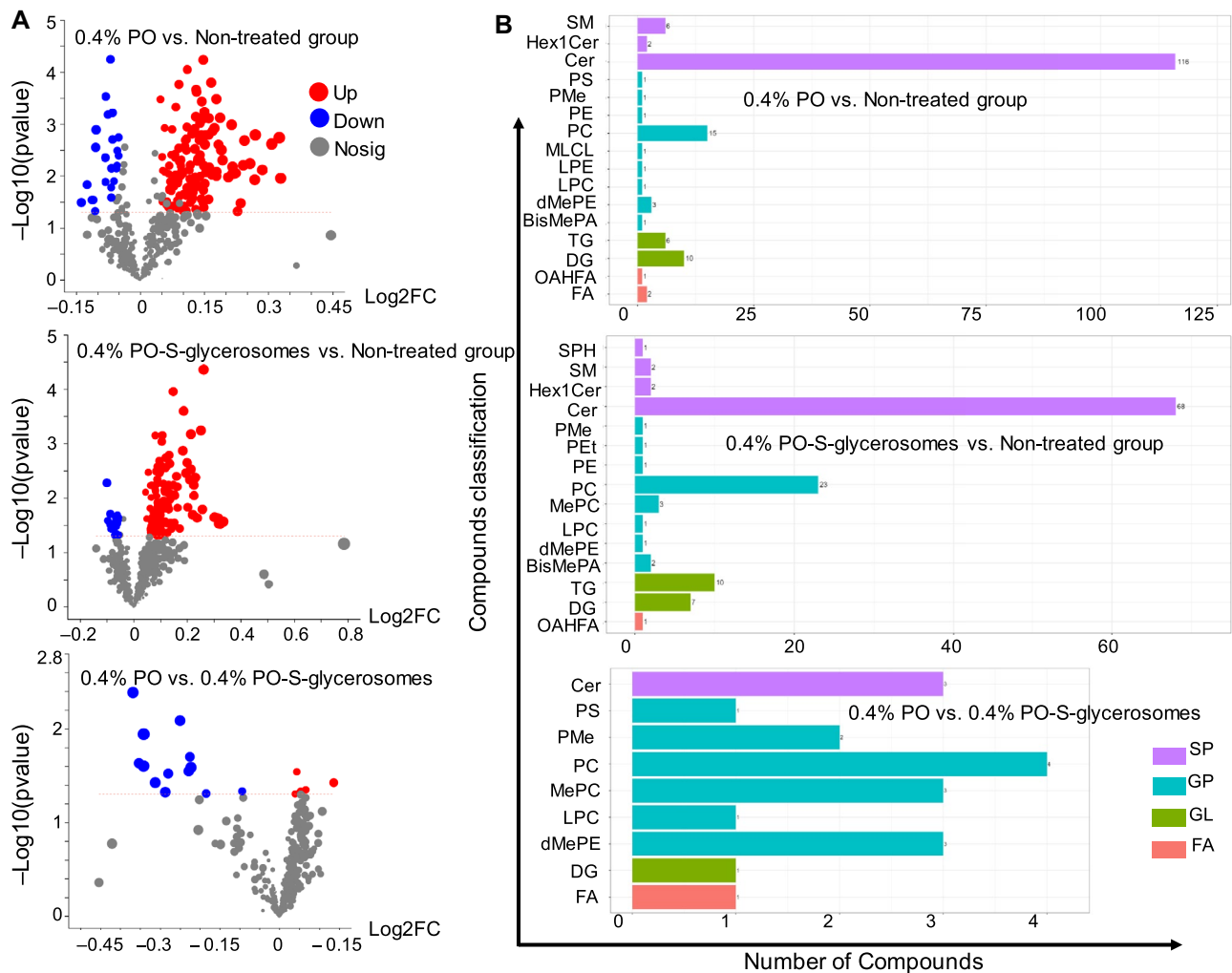


Fig. 7 Lipidomic analysis of the mouse stratum corneum. **A** Differential volcano plots: skin treated with 0.4% peppermint oil and 0.4% PO-S-glycerosomes significantly up- or downregulated the abundance of each lipid subclass in the skin compared to skin from the non-treated group. **B** Numerical maps of differential lipid compound subtypes:

treatment with 0.4% peppermint oil and 0.4% PO-S-glycerosomes altered the subtypes and amounts of sphingolipids (SPs), glycerophospholipids (GPs), glycerolipids (GLs), and fatty acids (FAs) in SC compared to the non-treated group ($n=5$)

the tested formulation did not induce significant skin irritation. However, the current results are only a preliminary assessment, and further investigation of the toxicity of the formulation including changes in the microstructure of the skin and monitoring of inflammation-related factors, as well as systemic toxicity and teratogenicity and mutagenicity, is required.

Discussion

LA possesses poor aqueous solubility and low bioavailability, thus limiting its clinical application. To address this issue, we prepared novel LA-loaded PO-S-glycerosomes

to improve the transdermal permeation and potential anti-inflammatory effect of LA.

Electrically neutral HSPC and SPC-100 are preferentially selected to form glycerosomes because the skin surface is negatively charged under physiological conditions; thus, positively charged glycerosomes readily penetrate into the deeper skin layer. However, the phase transition temperature of HSPC is 55 °C, thus requiring a higher hydration temperature and increasing the probability of oxidation. In contrast, the phase transition temperature of SPC-100 is -20 °C allowing it to be hydrated at moderate temperatures [32]. Thus, we selected SPC-100 as the phospholipid material.

Although cholesterol is often used as a stabilizer in the preparation of liposomes and ethosomes, its negative effects limit

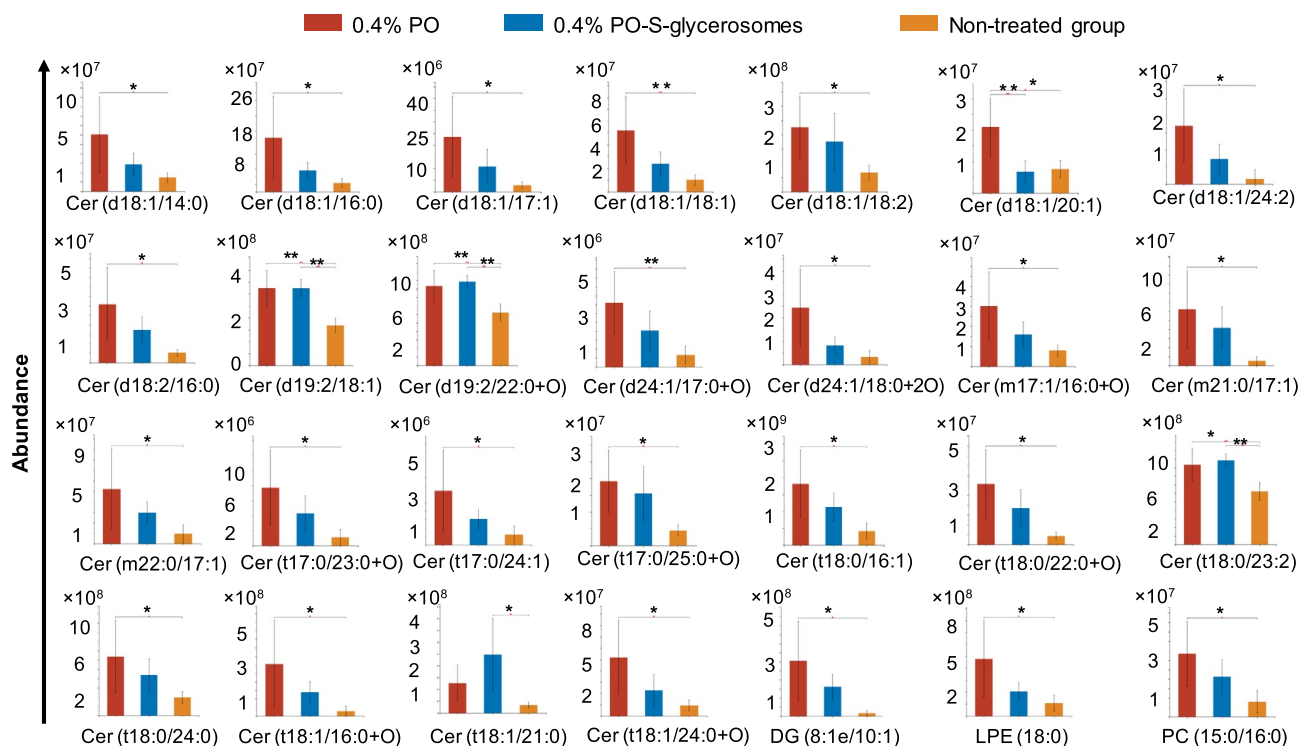


Fig. 8 Abundance of differential ceramides, glycerolipids, and glycerophospholipids in the stratum corneum of non-treated mice and treated with 0.4% peppermint oil and 0.4% PO-S-glycosomes. Values represented as the mean \pm standard deviation ($n=5$). ** $p < 0.01$, * $p < 0.05$

its clinical application. Meanwhile, sterols have been reported as potential alternative liposome stabilizers. In particular, plant-derived phytosterols have attracted increasing attention for their cholesterol-lowering effect in vivo [11]. During the liposomal storage, the membrane phospholipids can become oxidized leading to destruction of the lipid bilayer and drug leakage. However, liposomal stability is improved by phytosterols owing to their planar ring structure that interferes with phospholipid interactions. Thus, the phytosterol β -sitosterol exhibits superior effects on the stability of liposomes compared with that of cholesterol and stigmasterol [15]. In fact, Marsan et al. showed that β -sitosterol maximizes the van der Waals force between sitosterol and adjacent phospholipid

molecules, caused by the fully extended β -sitosterol side chain increasing the thickness of the hydrophobic layer [33]. As a result, β -sitosterol exhibits a stronger ability to control the arrangement of soybean phosphatidylcholine than stigmasterol. β -Sitosteryl sulfate also improves the dispersion of DPPC liposomes and enhance their hydration, thus increasing the fluidity of phospholipid membranes [34]. Accordingly, in our current work, β -sitosterol was selected as a stabilizer to avoid the potential in vivo side effects caused by cholesterol. The EE of the obtained nanocarriers for hydrophobic LA exceeded 70%, which was attributed to the formation of many liquid-ordered domains between the phospholipid membranes and β -sitosterol [35].

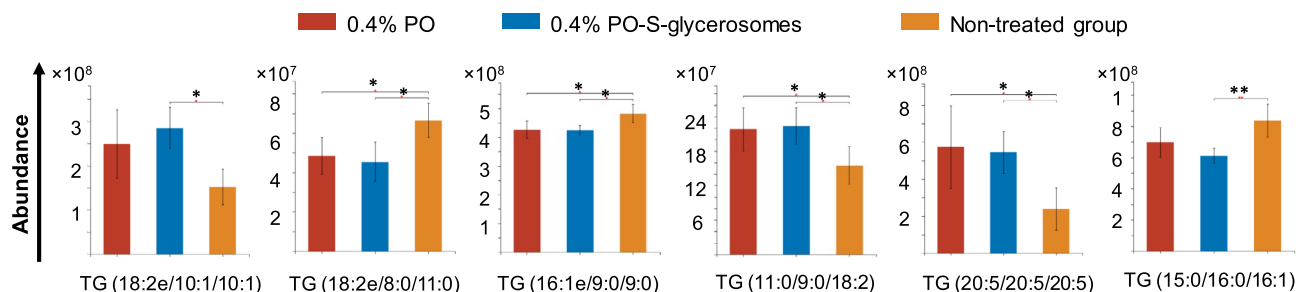


Fig. 9 Differential glycerolipid TG abundance in the stratum corneum of the non-treated mouse and mouse treated, respectively, with 0.4% peppermint oil and 0.4% PO-S-glycosomes. Values represented as the mean \pm standard deviation ($n=5$). ** $p < 0.01$, * $p < 0.05$

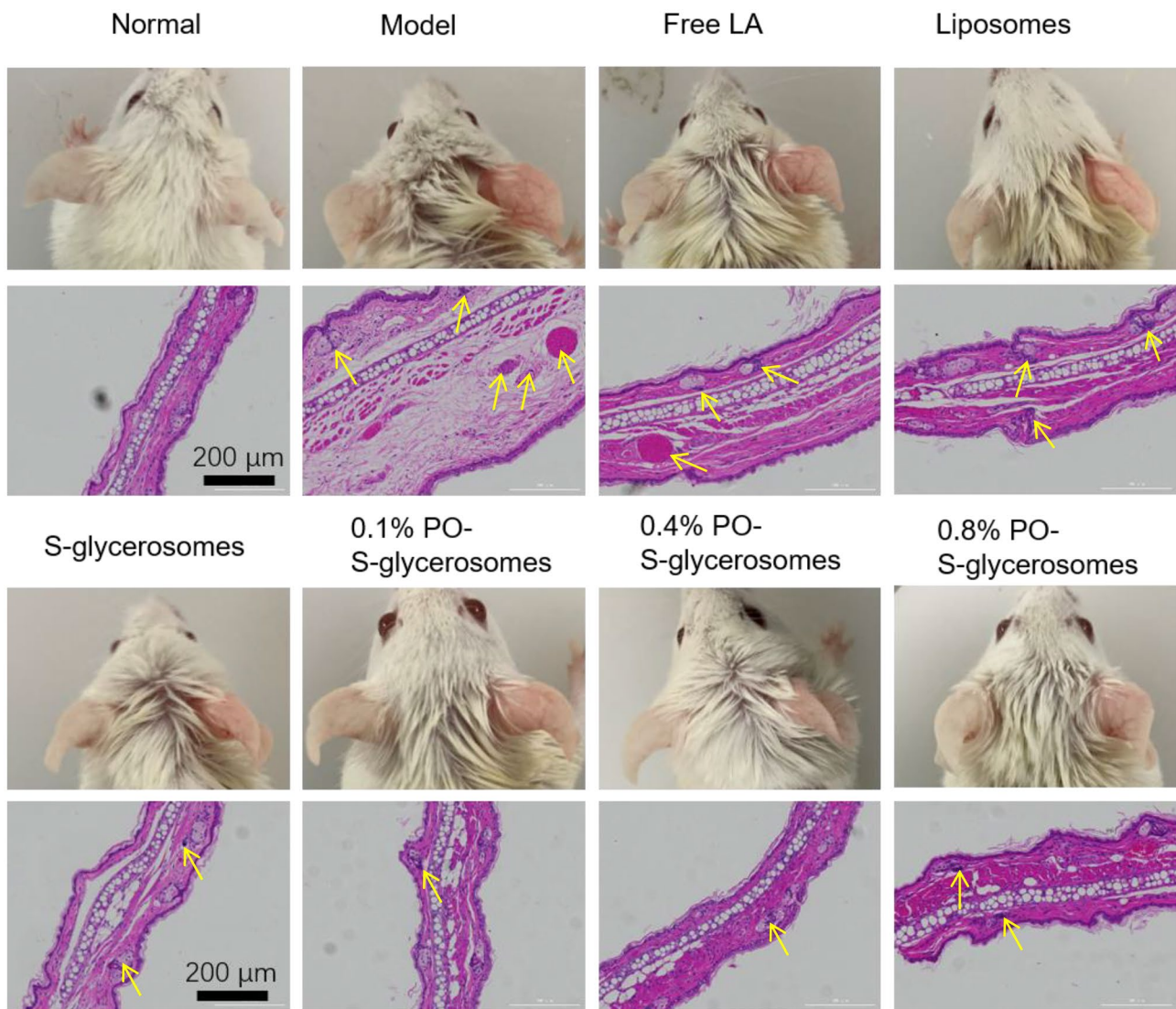


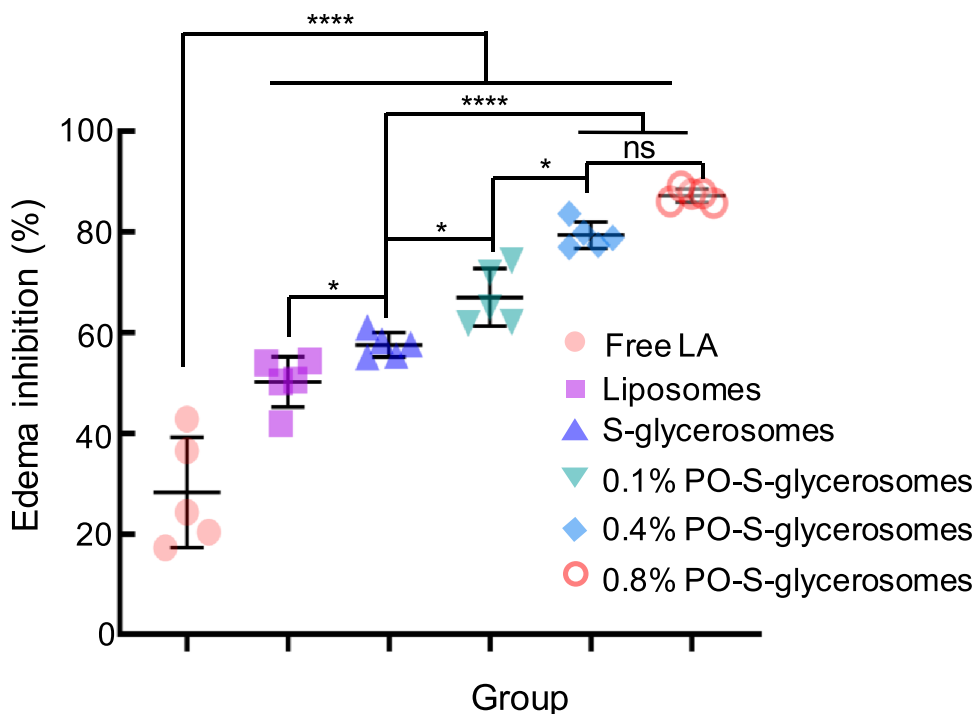
Fig. 10 Inhibition of xylene-induced ear swelling in mice treated with different preparations. Appearance of the ears and micrographs of H&E-stained sections of isolated ears of mice in different groups ($n=5$). Arrows indicate sites of edema, congestion, and inflammatory cell infiltration

The positive effect of the phospholipid content on EE is attributed to the lipophilicity of LA, which is more encapsulated within the internal phospholipid bilayers of particles with an increase in phospholipid content. This is consistent with the findings of Naguib et al., who showed that the EE of lacidipine increased with an increase in phospholipid concentration [27]. Moreover, in the current study, the EE increased with an increase in the drug to phospholipid ratio owing to the integration of LA in the phospholipid bilayer at a level that approached saturation. Meanwhile, the S-glycerosome particle size increased along with the glycerol proportion, possibly due to the glycerol reducing phospholipid bilayer rigidity, making it easier to gather into particles [7, 28]. Glycerol also increased the membrane permeability; thus, excessive glycerol concentrations

decreased the EE of S-glycerosomes (Fig. 2). However, β -sitosterol and β -sitosteryl sulfate have been shown to act as stabilizers to reduce the average particle size and unify the particle size distribution, while β -sitosteryl sulfate also protects liposomes from being reduced in size via sonication [34, 35]. Indeed, the S-glycerosomes formulated with the optimized conditions exhibited no significant changes in physicochemical properties after being stored at $4 \text{ }^{\circ}\text{C} \pm 2 \text{ }^{\circ}\text{C}$ for 3 days, with a mean size, zeta potential, EE, and DL of $148.70 \pm 3.82 \text{ nm}$ (PDI was 0.299 ± 0.042), $-4.31 \pm 0.20 \text{ mV}$, $71.36 \pm 0.83\%$, and $4.14 \pm 0.11\%$, respectively, exhibiting good overall physicochemical stability of the nano-dispersions.

LA-loaded PO-S-glycerosomes exhibited better transdermal flux than that of glycerosomes, liposomes, and free LA.

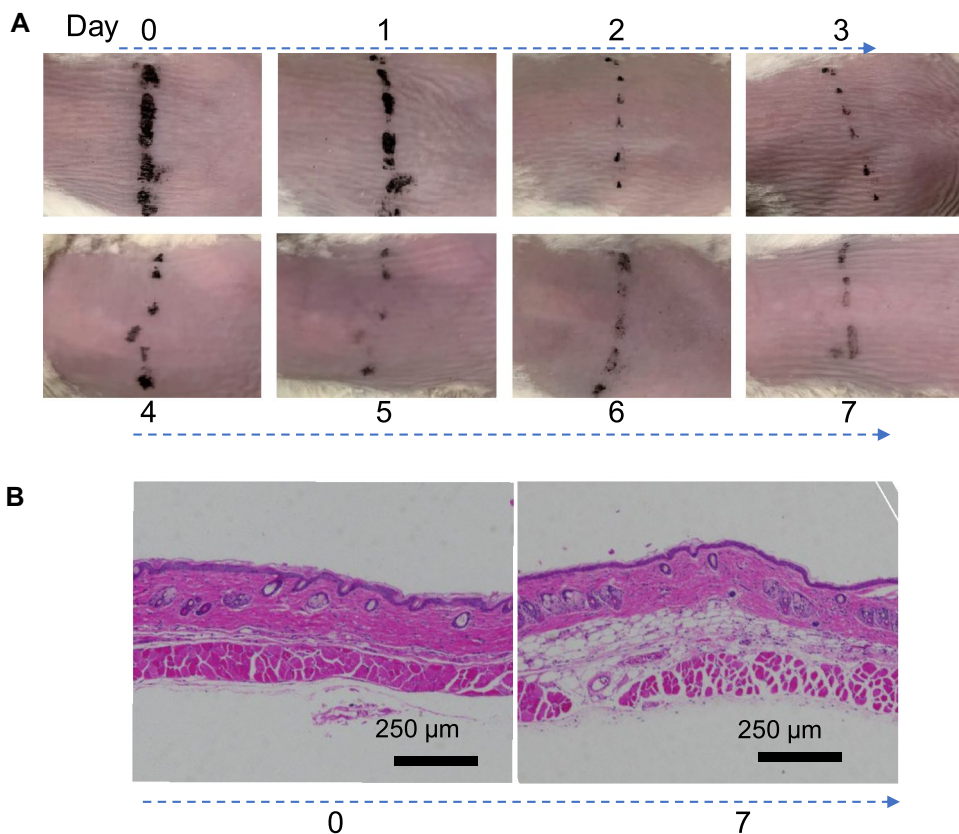
Fig. 11 Ear edema inhibition in mice treated with different preparations. Values represented as the mean \pm standard deviation ($n=5$). **** $p < 0.0001$, *** $p < 0.0001$, ** $p < 0.01$, * $p < 0.05$, ns: no significant difference



The transdermal flux of nanocarrier groups was superior to that of the free LA group owing to the high affinity of phospholipids in S-glycerosomes and liposomes for biofilms

[36]. Moreover, compared with liposomes, S-glycerosomes had a higher transdermal flux attributed to the addition of glycerol. Furthermore, the glycerol in glycerosomes altered

Fig. 12 Skin irritation evaluation of 0.4% PO-S-glycerosomes ($n=6$). **A** Appearance of mouse skin treated with 0.4% PO-S-glycerosome on days 0, 1, 2, 3, 4, 5, 6, and 7 (skin to the right of the demarcation line) and untreated skin (skin to the left of the demarcation line). **B** H&E staining of dorsal skin on days 0 and 10



the conformation of phospholipid headgroup in the SC from perpendicular to parallel to the membrane plane, altering the lipid structure in the SC and improving skin cell hydration, thus enhancing transdermal permeation [37–39]. More specifically, the released glycerol acts on the intercellular lipid bilayer of SC cells, resulting in partial extraction of intercellular lipids and partial transformation of solid lipids into liquid lipids. This leads to further disruption of the tight arrangement of the lipid bilayer [40]. Meanwhile, glycerol possesses –OH groups with stronger electronegativity than the –NH groups in ceramides, found in the SC and participating in hydrogen bonds. Therefore, glycerol can compete with the ceramide head group in the formation of hydrogen bonds, resulting in the destruction of the tight structure, and increasing the SC permeation, which is more conducive to transdermal delivery of LA [41].

Inclusion of low PO concentrations in the S-glycosomes dispersions enhanced transdermal permeation. The mechanisms by which volatile oils facilitate permeation include (a) altering the arrangement of SC and increasing the disturbance of the lipid skeleton and interstitial fluidity of SC; (b) influencing hydration of the SC by improving the ability of nitrogen compounds in skin keratin to combine with water, resulting in larger openings of sweat glands and hair follicles, increased skin aperture, and reduced resistance of the skin barrier to drug diffusion [17]; and (c) increasing the blood flow rate of skin capillaries, which promotes drug permeation across the SC to dermal capillaries [16]. Moreover, PO contains more than 28% menthol, which participates in thermodynamic interactions with cholesterol and ceramide components of the SC. That is, skin lipids melt at 75 °C, whereas menthol lowers the transition temperature of the SC, exhibiting greater effects with increased methanol content [42]. Menthol, as an alcoholic terpene, also has –OH groups, which synergistically compete with glycerol for hydrogen bonds in ceramides within the SC, thereby disrupting the tight structure [41]. We found that as the proportion of PO increased, the transdermal flux increased. However, the increasing trend gradually slowed at higher PO proportions and no longer exhibited dose dependence. This is likely attributed to the high concentration of volatile oils increasing the permeability of phospholipid membranes leading to drug leakage and enhanced transdermal delivery by nanocarriers. Meanwhile, the increase in volatile oil concentration would induce formation of a gel on the surface of glycosomes, increasing its viscosity and leading to the decreased permeation rate [43].

The greater the cumulative transdermal permeation and the faster the transdermal permeability, the more LA traverses the skin barrier to become released into the affected site. This ultimately leads to superior inhibition of edema. PO-S-glycosomes significantly increased the inhibition of edema via promotion of transdermal permeation. Moreover, menthol—the main component of PO—reportedly interferes with TRPA1 channels,

reducing skin pain, hypersensitivity, and neurogenic inflammation [44]. Activation of TRPA1 channels is associated with pain and development of inflammation through increased NO levels and Ca²⁺ concentration, which are related to the release of the relevant factors [45]. In addition, L-menthone inhibits the release of inflammatory cytokines, thus reducing their levels in vivo [46]. Thus, L-menthone can balance vasomotor abnormalities and decrease the inflammatory response, suggesting that PO acts synergistically with LA as an anti-inflammatory agent.

Conclusions

In this study, novel PO-S-glycosomes were developed as a carrier for the transdermal delivery of LA with β -sitosterol as a stabilizer, replacing the traditional cholesterol. S-glycosomes exhibited higher transdermal permeation efficiency compared to liposomes. Moreover, PO-S-glycosomes with 0.4% PO significantly weakened the barrier function of the SC to LA, resulting in a better anti-inflammatory response, in which PO acted synergistically with LA owing to its inherent anti-inflammatory and analgesic effects, achieving the unification of permeation enhancer and drug. Additionally, treatment with PO-S-glycosomes altered the isoform type, number, and content of SPs, GPs, GLs, and FAs in the SC, which may be associated with the permeation enhancement of PO-S-glycosomes. Taken together, this work demonstrates that PO-S-glycosomes can serve as a potential cholesterol-free carrier for transdermal therapy. However, due to the liquid properties of PO-S-glycosomes, which are not conducive to clinical administration, combining them with hydrogels may be an effective way to further dosage form improvement.

Acknowledgements We thank prof. Wei Wu from the School of Pharmacy, Fudan University, for providing P4 fluorescence probe.

Author contribution Conceptualization, N.F., Y.Z., and C.Z.; methodology, H.R. and L.S.; software, H.R.; validation, H.R., T.G., X.H., J.L., C.Z., and Y.Z.; formal Analysis, H.R.; investigation, C.Z. and Y.Z.; resources, N.F., C.Z., and Y.Z.; data curation, H.R.; writing, original draft preparation, H.R.; writing, review and editing, Y.Z.; visualization, N.F.; supervision, N.F. C.Z., and Y.Z.; project administration, H.R. and L.S.; funding acquisition, C.Z., Y.Z., and N.F.; Y.Z., N.F., and Y.Z. are co-corresponding authors.

Funding This work was supported by the National Natural Science Foundation of China (Grant number 82074031), the Program for Professor of Special Appointment (Eastern Scholar) at Shanghai Institutions of Higher Learning (Grant number TP2020054), and the Program for Shanghai High-Level Local University Innovation Team (SZY20220315).

Availability of data and materials The datasets generated during and analyzed during the current study are available from the corresponding author upon reasonable request.

Declarations

Ethics approval The laboratory animal license number is SYXK (SH) 2020–0009. All procedures in the experiments followed the Experimental Animal Welfare and Ethics Committee guidelines.

Consent to participate Not applicable.

Consent for publication Not applicable.

Competing interests The authors declare no competing interests.

References

- Pang L, Liu CY, Gong GH, et al. Synthesis, in vitro and in vivo biological evaluation of novel lappaconitine derivatives as potential anti-inflammatory agents. *Acta Pharm Sin B*. 2020;10(4):628–45.
- Teng G, Zhang X, Zhang C, et al. Lappaconitine trifluoroacetate contained polyvinyl alcohol nanofibrous membranes: characterization, biological activities and transdermal application. *Mater Sci Eng C Mater Biol Appl*. 2020;108: 110515.
- Horwitz E, Pisanty S, Czerninski R, et al. A clinical evaluation of a novel liposomal carrier for acyclovir in the topical treatment of recurrent herpes labialis. *Oral Surg Oral Med Oral Pathol Oral Radiol Endod*. 1999;87(6):700–5.
- Touitou E, Dayan N, Bergelson L, et al. Ethosomes - novel vesicular carriers for enhanced delivery: characterization and skin penetration properties. *J Control Release*. 2000;65(3):403–18.
- Paiva-Santos AC, Silva AL, Guerra C, et al. Ethosomes as nano-carriers for the development of skin delivery formulations. *Pharm Res*. 2021;38(6):947–70.
- Touitou E, Natsheh H. Topical administration of drugs incorporated in carriers containing phospholipid soft vesicles for the treatment of skin medical conditions. *Pharmaceutics*. 2021;13(12):2129.
- Manca ML, Zaru M, Manconi M, et al. Glycerosomes: a new tool for effective dermal and transdermal drug delivery. *Int J Pharm*. 2013;455(1–2):66–74.
- Kaddah S, Khreich N, Kaddah F, et al. Cholesterol modulates the liposome membrane fluidity and permeability for a hydrophilic molecule. *Food Chem Toxicol*. 2018;113:40–8.
- Tall AR, Yvan-Charvet L. Cholesterol, inflammation and innate immunity. *Nat Rev Immunol*. 2015;15(2):104–16.
- Srihera N, Li Y, Zhang TT, et al. Preparation and characterization of astaxanthin-loaded liposomes stabilized by sea cucumber sulfated sterols instead of cholesterol. *J Oleo Sci*. 2022;71(3):401–10.
- Tai K, Liu F, He X, et al. The effect of sterol derivatives on properties of soybean and egg yolk lecithin liposomes: stability, structure and membrane characteristics. *Food Res Int*. 2018;109:24–34.
- Zhang R, Han Y, McClements DJ, et al. Production, characterization, delivery, and cholesterol-lowering mechanism of phytosterols: a review. *J Agric Food Chem*. 2022;70(8):2483–94.
- Salehi B, Quispe C, Sharifi-Rad J, et al. Phytosterols: from pre-clinical evidence to potential clinical applications. *Front Pharmacol*. 2021;11: 599959.
- Han C, Yang C, Li X, et al. DHA loaded nanoliposomes stabilized by β -sitosterol: preparation, characterization and release in vitro and vivo. *Food Chem*. 2022;368: 130859.
- Lee DU, Park HW, Lee SC. Comparing the stability of retinol in liposomes with cholesterol, β -sitosterol, and stigmaterol. *Food Sci Biotechnol*. 2021;30(3):389–94.
- Zhou W, He S, Yang Y, et al. Formulation, characterization and clinical evaluation of propranolol hydrochloride gel for transdermal treatment of superficial infantile hemangioma. *Drug Dev Ind Pharm*. 2015;41(7):1109–19.
- Williams AC, Barry BW. Terpenes and the lipid-protein-partitioning theory of skin penetration enhancement. *Pharm Res*. 1991;8(1):17–24.
- Zhang K, Zhang Y, Li Z, et al. Essential oil-mediated glycerosomes increase transdermal paeoniflorin delivery: optimization, characterization, and evaluation in vitro and in vivo. *Int J Nanomedicine*. 2017;12:3521–32.
- Zhang Y, Zhang H, Zhang K, et al. Co-hybridized composite nanovesicles for enhanced transdermal eugenol and cinnamaldehyde delivery and their potential efficacy in ulcerative colitis. *Nanomedicine*. 2020;28: 102212.
- Guo T, Zhang Y, Zhao J, et al. Nanostructured lipid carriers for percutaneous administration of alkaloids isolated from *Aconitum sinomontanum*. *J Nanobiotechnology*. 2015;13:47.
- Wang YZ, Ren TC, Xiao YQ. Effects of different penetration enhancers on percutaneous absorption of lappaconitine gel in vitro. *Zhongguo Zhong Yao Za Zhi*. 2005;30(9):665–8.
- Siddoju S, Sachdeva V, Friden PM, et al. Acyclovir skin depot characterization following in vivo iontophoretic delivery. *Skin Res Technol*. 2011;17(2):234–44.
- Saini RK, Prasad P, Shang X, et al. Advances in lipid extraction methods-a review. *Int J Mol Sci*. 2021;22(24).
- Matyash V, Liebis G, Kurzchalia TV, et al. Lipid extraction by methyl-tert-butyl ether for high-throughput lipidomics. *J Lipid Res*. 2008;49(5):1137–46.
- Wang YZ, Xiao YQ, Zhang C, et al. Study of analgesic and anti-inflammatory effects of lappaconitine gelata. *J Tradit Chin Med*. 2009;29(2):141–5.
- Saito A, Tanaka H, Usuda H, et al. Characterization of skin inflammation induced by repeated exposure of toluene, xylene, and formaldehyde in mice. *Environ Toxicol*. 2011;26(3):224–32.
- Naguib MJ, Salah S, Abdel Halim SA, et al. Investigating the potential of utilizing glycerosomes as a novel vesicular platform for enhancing intranasal delivery of lacidipine. *Int J Pharm*. 2020;582: 119302.
- Taladrid D, Marín D, Alemán A, et al. Effect of chemical composition and sonication procedure on properties of food-grade soy lecithin liposomes with added glycerol. *Food Res Int*. 2017;100(Pt 1):541–50.
- Su R, Fan W, Yu Q, et al. Size-dependent penetration of nanoemulsions into epidermis and hair follicles: implications for transdermal delivery and immunization. *Oncotarget*. 2017;8(24):38214–26.
- Kumar A, Pathak K, Bali V. Ultra-adaptable nanovesicular systems: a carrier for systemic delivery of therapeutic agents. *Drug Discov Today*. 2012;17(21–22):1233–41.
- Gu S, Gao J, Hou X, et al. Effects of penetration enhancers on shuangwu traumatic formula: in vitro percutaneous absorption and in vivo pharmacodynamic evaluation of an herb medicine. *Eur J Pharm Biopharm*. 2009;73(3):385–90.
- López-Pinto JM, González-Rodríguez ML, Rabasco AM. Effect of cholesterol and ethanol on dermal delivery from DPPC liposomes. *Int J Pharm*. 2005;298(1):1–12.
- Marsan MP, Bellet-Amalric E, Muller I, et al. Plant sterols: a neutron diffraction study of sitosterol and stigmaterol in soybean phosphatidylcholine membranes. *Biophys Chem*. 1998;75(1):45–55.
- Kafle A, Akamatsu M, Bhadani A, et al. Effects of β -sitosterol sulfate on the properties of DPPC liposomes. *J Oleo Sci*. 2018;67(12):1511–9.
- Tai K, Rappolt M, He X, et al. Effect of β -sitosterol on the curcumin-loaded liposomes: vesicle characteristics, physicochemical

- stability, in vitro release and bioavailability. *Food Chem.* 2019;293:92–102.
36. Li J, Tan T, Zhao L, et al. Recent advancements in liposome-targeting strategies for the treatment of gliomas: a systematic review. *ACS Appl Bio Mater.* 2020;3(9):5500–28.
 37. Barichello JM, Yamakawa N, Kisyuku M, et al. Combined effect of liposomalization and addition of glycerol on the transdermal delivery of isosorbide 5-nitrate in rat skin. *Int J Pharm.* 2008;357(1–2):199–205.
 38. Westh P. Unilamellar DMPC vesicles in aqueous glycerol: preferential interactions and thermochemistry. *Biophys J.* 2003;84(1):341–9.
 39. Terakosolphan W, Trick JL, Royall PG, et al. Glycerol solvates DPPC headgroups and localizes in the interfacial regions of model pulmonary interfaces altering bilayer structure. *Langmuir.* 2018;34(23):6941–54.
 40. Jain S, Tiwary AK, Sapra B, et al. Formulation and evaluation of ethosomes for transdermal delivery of lamivudine. *AAPS Pharm-SciTech.* 2007;8(4):E111.
 41. Jain AK, Thomas NS, Panchagnula R. Transdermal drug delivery of imipramine hydrochloride. I. Effect of terpenes. *J Control Release.* 2002;79(1–3):93–101.
 42. Kaplun-Frischoff Y, Touitou E. Testosterone skin permeation enhancement by menthol through formation of eutectic with drug and interaction with skin lipids. *J Pharm Sci.* 1997;86(12):1394–9.
 43. Zhang YT, Zhao JH, Zhang SJ, et al. Enhanced transdermal delivery of evodiamine and rutaecarpine using microemulsion. *Int J Nanomedicine.* 2011;6:2469–82.
 44. Andersen HH, Gazerani P, Arendt-Nielsen L. High-concentration L-menthol exhibits counter-irritancy to neurogenic inflammation, thermal and mechanical hyperalgesia caused by trans-cinnamaldehyde. *J Pain.* 2016;17(8):919–29.
 45. Yuan R, Zhang D, Yang J, et al. Review of aromatherapy essential oils and their mechanism of action against migraines. *J Ethnopharmacol.* 2021;265: 113326.
 46. Xue J, Li H, Deng X, et al. L-Menthone confers antidepressant-like effects in an unpredictable chronic mild stress mouse model via NLRP3 inflammasome-mediated inflammatory cytokines and central neurotransmitters. *Pharmacol Biochem Behav.* 2015;134:42–8.

Publisher's Note Springer Nature remains neutral with regard to jurisdictional claims in published maps and institutional affiliations.

Springer Nature or its licensor (e.g. a society or other partner) holds exclusive rights to this article under a publishing agreement with the author(s) or other rightsholder(s); author self-archiving of the accepted manuscript version of this article is solely governed by the terms of such publishing agreement and applicable law.